ELSEVIER

Contents lists available at ScienceDirect

# Earth and Planetary Science Letters

www.elsevier.com/locate/epsl



# Spatio-temporal evolution of Australasian monsoon hydroclimate over the last 40,000 years



Claire E. Krause <sup>a,\*</sup>, Michael K. Gagan <sup>a,b</sup>, Gavin B. Dunbar <sup>c</sup>, Wahyoe S. Hantoro <sup>d,b</sup>, John C. Hellstrom <sup>e</sup>, Hai Cheng <sup>f,g</sup>, R. Lawrence Edwards <sup>f</sup>, Bambang W. Suwargadi <sup>d</sup>, Nerilie J. Abram <sup>a,h</sup>, Hamdi Rifai <sup>i</sup>

- <sup>a</sup> Research School of Earth Sciences, The Australian National University, Canberra, ACT 2601, Australia
- <sup>b</sup> School of Earth and Environmental Sciences, The University of Queensland, Brisbane, Qld 4072, Australia
- <sup>c</sup> Antarctic Research Centre, Victoria University of Wellington, Wellington 6140, New Zealand
- <sup>d</sup> Research Center for Geotechnology, Indonesian Institute of Sciences, Bandung 40135, Indonesia
- <sup>e</sup> School of Earth Sciences, The University of Melbourne, Parkville, Vic. 3010, Australia
- f Department of Earth Sciences, University of Minnesota, Minneapolis, MN 55455, USA
- <sup>g</sup> Institute of Global Environmental Change, Xi'an Jiatong University, Xi'an 710049, China
- <sup>h</sup> ARC Centre of Excellence for Climate Extremes, The Australian National University, Canberra, ACT 2601, Australia
- <sup>i</sup> Department of Physics, State University of Padang, Padang 25131, Indonesia

#### ARTICLE INFO

# Article history: Received 1 September 2018 Received in revised form 22 January 2019 Accepted 25 January 2019 Available online 4 March 2019 Editor: D. Vance

Keywords: Indonesia speleothem oxygen isotopes Australasian monsoon Maritime Continent

# ABSTRACT

Maritime Continent (MC) convection drives zonal and meridional climate modes, including the Australasian monsoon system, but its role in past global climate change remains uncertain. Here we use speleothem oxygen isotope ( $\delta^{18}$ O) records from a latitudinal transect across the MC, and a new critically located record for southwest Sulawesi, Indonesia, to reconstruct spatial hydroclimate variability in the Australasian monsoon domain over the last 40,000 yr. Our results show that atmospheric convection in the core MC region was reduced from  $\sim$ 40,000 to 12,000 yr ago and strengthened rapidly only after the inundation of shallow continental shelves in the region, well after the onset of deglaciation. Interestingly, the millennial-scale climatic impacts of North Atlantic Heinrich events are not evident in Sulawesi. Together with climate model simulations, we demonstrate that changes in deep atmospheric convection dominate glacial–interglacial hydroclimate over the MC, whereas latitudinal shifts in the mean location of the InterTropical Convergence Zone control rainfall patterns during abrupt climate changes.

# 1. Introduction

Deep atmospheric convection over the western equatorial Pacific is critical for the redistribution of energy and moisture within Earth's climate system (e.g., Webster, 1994). This convection is driven by evaporation of the warm waters of the Indo-Pacific Warm Pool (>28°C), and is vital for the global heat transport from the equator to the poles (Schneider et al., 2014). Western equatorial Pacific convection drives zonal and meridional climate modes, including the dynamic Australasian monsoon system (e.g., Chiang, 2009). Latitudinal movements of the region of maximum convective rainfall over the western equatorial Pacific form part of the global Intertropical Convergence Zone (ITCZ), which acts

E-mail address: claire.krause@ga.gov.au (C.E. Krause).

as Earth's meteorological equator. The seasonal migration of the ITCZ, and associated seasonal reversals of the Australasian monsoon (incorporating the East Asian summer monsoon (EASM) and Indo-Australian summer monsoon (IASM)) determine the distribution and timing of rainfall throughout the tropics and subtropics of Australasia (Webster et al., 1998) (Fig. 1). The combined effect of deep atmospheric convection and the large latitudinal sweep of the ITCZ make the Australasian monsoon domain the most atmospherically dynamic region on Earth.

Crown Copyright © 2019 Published by Elsevier B.V. All rights reserved.

Speleothem records from the northern and southern regions of the Australasian monsoon document anti-phased rainfall responses to orbital precessional insolation forcing and millennial-scale climate events, interpreted as latitudinal shifts in the mean location of the ITCZ (Ayliffe et al., 2013; Denniston et al., 2013; Griffiths et al., 2009; Lewis et al., 2011; Wang et al., 2001); noting that differing interpretations of Chinese speleothem records have been proposed by a number of authors (see Zhang et al., 2018, and references therein). Records from the core of the west-

<sup>\*</sup> Corresponding author. Now at Geoscience Australia, Canberra, Australian Capital Territory, 2601, Australia.

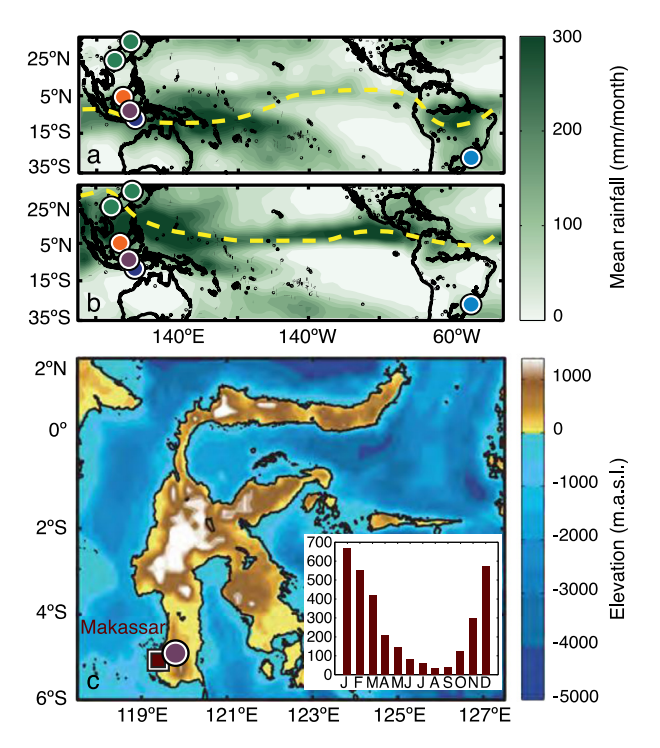


**Fig. 1. Location map showing tropical Pacific hydroclimate.** Mean January (a) and July (b) rainfall for the period 1979–2014. Dashed yellow lines show the approximate location of the ITCZ. Circles in (a)–(b) indicate the locations of speleothem records for Hulu and Dongge caves, China (green) (Dykoski et al., 2005; Wang et al., 2001); Gunung Buda, Borneo (orange) (Carolin et al., 2013; Partin et al., 2007); Liang Luar Cave, Flores (dark blue) (Ayliffe et al., 2013; Griffiths et al., 2009; Lewis et al., 2011); Botuverá Cave, Brazil (light blue) (Wang et al., 2007) and Gempa Bumi Cave, Sulawesi (purple; this study). (c) Elevation of Sulawesi, Indonesia (in metres above sea level) with the locations of Gempa Bumi Cave (purple circle), the nearest major town, Makassar (maroon square), and monthly mean rainfall recorded at Makassar (inset). (For interpretation of the colours in the figure(s), the reader is referred to the web version of this article.)

ern equatorial Pacific, suggest that reduced rainfall coeval with Heinrich events may indicate reduced convective activity over the western equatorial Pacific (Carolin et al., 2013; Partin et al., 2007; Russell et al., 2014). Changes in the strength of deep atmospheric convection have implications for total rainfall received, whereas shifts in the ITCZ influence rainfall distribution; therefore, it is of critical importance to document the interaction of these processes in the past to fully understand the role of the Australasian monsoon in global climate.

The lack of continuous, highly resolved climate records from the IASM domain prevents the development of a regional picture of the behaviour of this monsoon system. Our understanding of the relationship between North Atlantic climate events and the western equatorial Pacific, as well as the relative behaviour of the EASM and IASM, will be explored in more detail using a well-dated climate record from Sulawesi, Indonesia. The location of Gempa Bumi Cave at 5°S, 119°E in Sulawesi allows us to study changes in IASM strength, ITCZ location and Indo-Pacific Warm Pool (IPWP) dynamics. It is well placed geographically between published speleothem records from Borneo and Flores (Fig. 1) to further develop our understanding of the migration of the monsoon and its response to North Atlantic climate forcings.

# 2. Materials and methods

# 2.1. Stalagmite collection and <sup>230</sup>Th dating

We present a  $^{230}$ Th-dated speleothem  $\delta^{18}$ O record for southwest Sulawesi, Indonesia, extending back continuously to 40 kyr BP

(thousand years before present; where present is 1950CE) (Fig. 1c, Fig. 2; Methods). Stalagmite GB09-3 (Fig. 2) was collected ~300 m from the entrance of Gempa Bumi cave (5°S, 120°E, 140 m above sea level) in the Maros limestone district of southwest Sulawesi, Indonesia. Rainfall over southwest Sulawesi is highly seasonal, with the Indo-Australian summer monsoon bringing ~80% of annual rainfall between November and March (Fig. 1c). This new record is optimally located to record changes in the strength of deep atmospheric convection over the MC. It also fills a critical gap in speleothem palaeoclimate records and allows us to reconstruct the latitudinal structure of hydroclimate variability on orbital and millennial time scales across the entire Australasian monsoon domain.

Stalagmite GB09-3 has a length of  $\sim$ 700 mm and an average diameter of  $\sim$ 50 mm (Fig. 2). Stalagmite GB11-9 was collected in 2011 from Gempa Bumi Cave to demonstrate replication of the isotope record across its interval of overlap with the older glacial section of GB09-03. Stalagmite GB11-9 has a length of  $\sim$ 615 mm and an average diameter of  $\sim$ 80 mm (Fig. 3). Both samples were not actively growing at the time of collection.

A total of 36 samples were analysed for uranium and thorium isotopes to develop the chronology for GB09-3. Six samples were analysed at the University of Minnesota, with the remaining 30 samples analysed at the University of Melbourne. Eight <sup>230</sup>Th dates for GB11-9 were analysed at the University of Melbourne. Dates were taken adjacent to the stable isotope sampling track, with an average sample size of 65 mg. Samples were analysed using multi-collector coupled plasma mass spectrometry (MC-ICP-MS), following the methods of Hellstrom (2003). All samples were corrected for detrital thorium using an initial [230Th/232Th] ratio of  $3.0\pm0.75$ . This value was determined using a Monte Carlo analysis on stratigraphic constraints on measured ages (Hellstrom, 2006), and represents the most likely initial thorium value for Sulawesi, based on the available ages of GB09-3. This value resulted in an average age correction of GB09-3 of 3% for ages older than 10 kyr BP, and 9% for all ages (note that the correction has the largest effect on younger dates, where the ratio of <sup>230</sup>Th/<sup>232</sup>Th is smaller). Dating samples from GB11-9 contained lower levels of detritus, with the detrital correction only resulting in an average age correction of 0.1%.

Age models were created using the Monte Carlo technique of Hellstrom (2006), which aligns <sup>230</sup>Th dates (corrected for detrital thorium) within their errors to ensure that they are in stratigraphic order. Two <sup>230</sup>Th ages were excluded from the age model of GB09-3: GB09-3-2 and GB09-3-uD6 (Fig. 2). Both of these samples had very large relative errors due to high detrital thorium (130% and 11% respectively. N.B. GB09-3-2 was the stalagmite top date) and were inconsistent with surrounding dates. When these two ages were excluded, the remaining age model had all dates in stratigraphic sequence, with no determinable hiatuses (Fig. 2). The mean growth rate for GB09-3 over the period 40–0 kyr BP was 0.9 mm per 50 yr.

The age model for GB11-9 comprises eight <sup>230</sup>Th ages, all in stratigraphic order, within error. All eight dates were used in the final age model, which was produced using the same Monte Carlo method as for GB09-3. The mean growth rate for GB11-9 over the period 40–23 kyr BP was 0.7 mm per 50 yr (Fig. 3).

## 2.2. Stable isotope analysis and error reporting

GB09-3 was continuously sampled for stable isotope analysis at an average interval of 0.9 mm ( $\sim$ 50 yr resolution) along the central growth axis. Stable isotope analysis was conducted on 755 samples, with an average sample size of 200 µg. Measurements of  $\delta^{18}$ O and  $\delta^{13}$ C were made at The Australian National University using a Finnigan MAT-251 mass spectrometer coupled to an automated Kiel carbonate device. GB11-9 was slabbed about the central

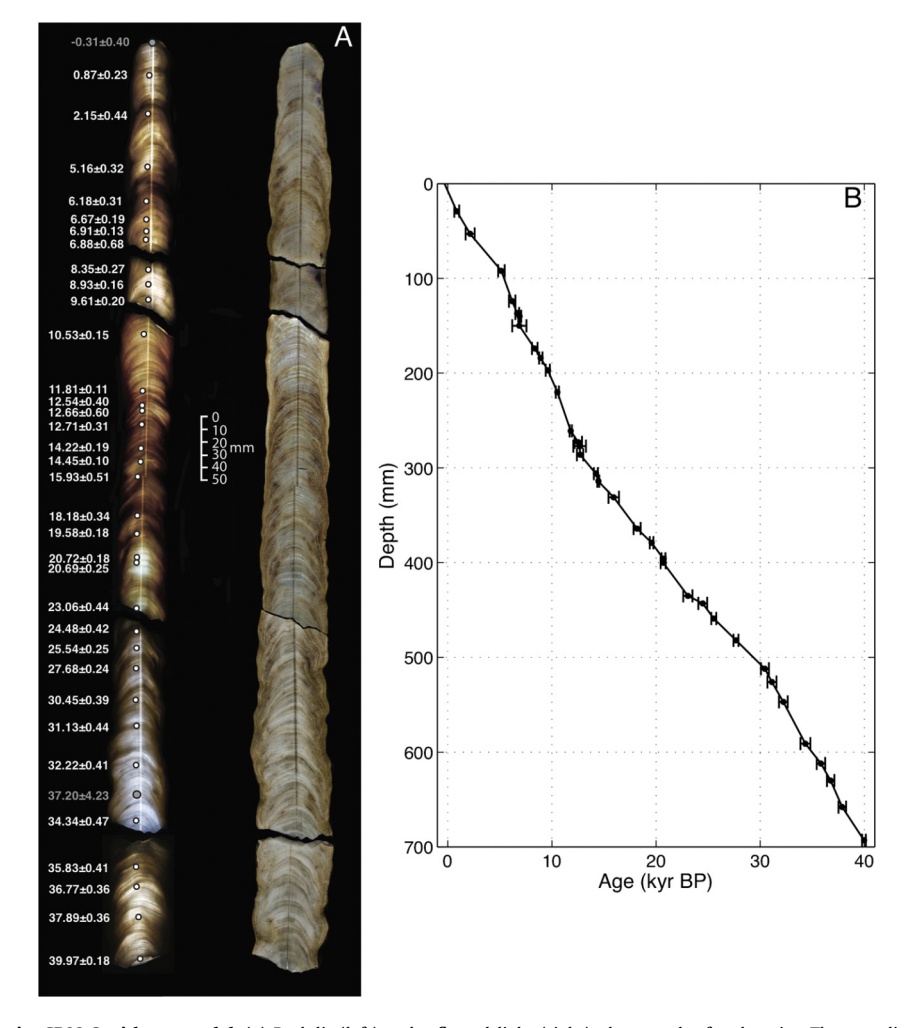


**Fig. 2. Photographs of stalagmite GB09-3 with age model.** (a) Back-lit (left) and reflected light (right) photograph of stalagmite. The sampling track used for stable isotope analysis is visible down the centre of the stalagmite. White dots show the locations of <sup>230</sup>Th dates, expressed as kyr BP (where present is defined as 1950 CE). Two dates shown in grey were not used in the final age model. Details of the <sup>230</sup>Th age data are given in Supplementary Table 1. (b) Age-depth plot for GB09-3. All ages are in stratigraphic sequence, within error. The mean growth rate for GB09-3 is 0.9 mm per 50 yr, with no determinable hiatuses.

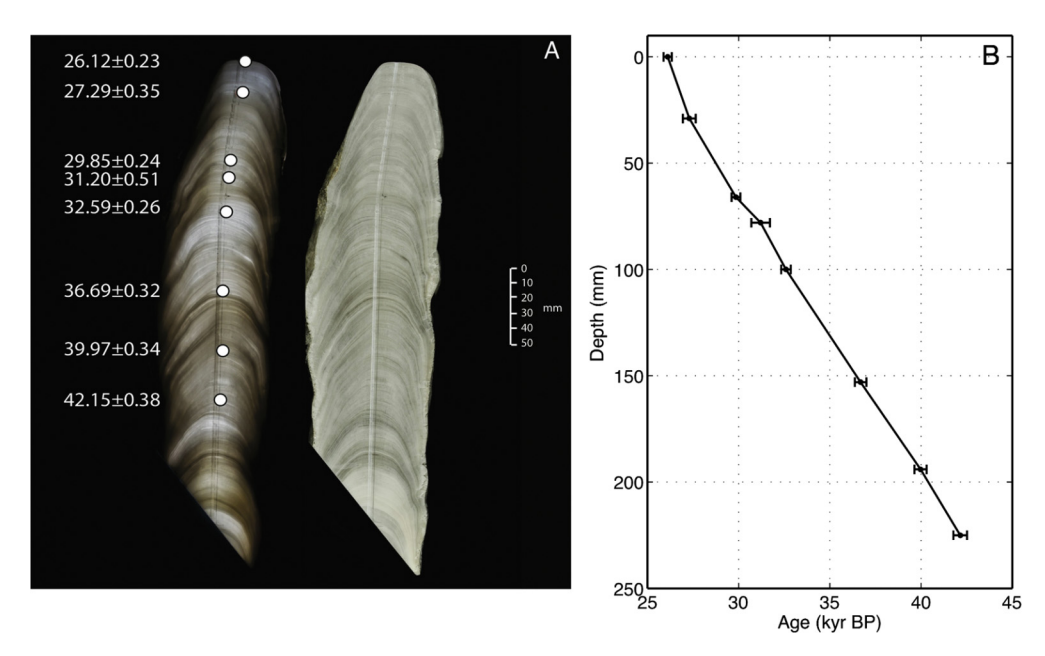


**Fig. 3. Photographs of stalagmite GB11-9 with age model.** (a) Back-lit (left) and reflected light (right) photograph of stalagmite. Sampling track used for stable isotope analysis is visible down the centre of the stalagmite. White dots show the locations of <sup>230</sup>Th dates, expressed as kyr BP (where present is defined as 1950 CE). Details of the <sup>230</sup>Th age data are given in Supplementary Table 1. (b) Age-depth plot for GB11-9. All ages are in stratigraphic sequence, within error. The mean growth rate for GB11-9 over the period 40–26 kyr BP is 0.7 mm per 50 yr, with no determinable hiatuses. Data from the lower section of GB11-9 are not included in this study.

growth axis and micromilled along the central axis using a 1-mm diameter drill bit at an interval of 0.7 mm, equating at an average sampling interval of  $\sim\!\!50$  yr. Analysis of  $\delta^{18}{\rm O}$  and  $\delta^{13}{\rm C}$  was conducted on a total of 323 samples.

For the isotope analysis, one NBS-19 standard was analysed for every 5–8 samples to ensure consistency among runs. Results are reported relative to Vienna Peedee Belemnite (VPDB) following adjustment using the in-run measurements of NBS-19 ( $\delta^{18}$ O = -2.20%) and less frequent measurements of NBS-18 ( $\delta^{18}$ O = -23.0%). The analytical error for measurements of NBS-19 was calculated by finding the standard deviation of NBS-19 across all runs. Using this method, the analytical error for NBS-19  $\delta^{18}$ O was 0.05% ( $n=187,\ 1\sigma$ ) for GB09-3, and 0.04% ( $n=83,\ 1\sigma$ ) for GB11-9.

The reproducibility of  $\delta^{18}$ O for the stalagmite samples themselves was determined by running duplicate and triplicate measurements. Samples with a run standard deviation greater than 0.05‰ (in  $\delta^{18}$ O) were re-run, in order to minimise error related to analysis methods. Additionally,  $\delta^{18}$ O values that deviated largely from adjacent values in the time series were duplicated to ensure that abrupt peaks and troughs in the data set reflect real changes in speleothem  $\delta^{18}$ O. Triplicates were run where duplicate measurements differed by more than 0.1‰ in  $\delta^{18}$ O. The mean standard error for duplicate/triplicate analyses of  $\delta^{18}$ O was 0.05‰ (n=126) for GB09-3 and 0.03‰ (n=46) for GB11-9.

# 2.3. Hosing model experiments

Heinrich events one (H1; 17 kyr BP), two (H2; 24 kyr BP) and three (H3; 32 kyr BP) were simulated using idealised hosing experiments in HadCM3 (Singarayer and Valdes, 2010). These were initialised from pre-industrial conditions, and forced with time appropriate orbital, greenhouse gas and ice sheet (including sea level) conditions. A model/proxy study of the LGM demonstrated the skill of HadCM3 in modelling conditions across the IPWP during the LGM compared to other models participating in the Paleoclimate Modelling Intercomparison Project, supporting the use of this model to examine past climate conditions over the IPWP (DiNezio and Tierney, 2013).

The equilibrium time slice runs for 17, 24 and 32 kyr BP were hosed to simulate a Heinrich event. The experimental design follows the PMIP protocol established in Stouffer et al. (2006), with one Sverdrup (1 Sv =  $1 \times 10^6 \text{ m}^3 \text{ s}^{-1}$ ) of freshwater continuously added to the surface of the North Atlantic between  $50^\circ \text{N}$  and  $70^\circ \text{N}$  latitude for 200 model years. HadCM3 has been found to be a relatively stable model, only displaying small anomalies in response to the more realistic freshwater forcing of 0.1 Sv, also used within PMIP (Kageyama et al., 2013; Stouffer et al., 2006). For this reason, we use the 1 Sv experiment for our analysis, as this forcing scenario best replicates the conditions recorded in proxy records during a Heinrich event, however we recognise that this experiment is idealised and not reflective of realistic Heinrich forcing (Deschamps et al., 2012; Fairbanks, 1989).

One Sv of freshwater added to the North Atlantic causes a large perturbation of the model AMOC (Singarayer and Valdes, 2010) and a southward shift of the model ITCZ, in line with proxy data. The model was allowed to equilibrate, and the results presented represent a climatology for the last 30 yr of each simulation. Full details of the experimental set up can be found in Singarayer and Valdes (2010).

# 3. Results

# 3.1. Interpretation of Sulawesi speleothem oxygen isotopes

We interpret changes in Sulawesi speleothem  $\delta^{18}O$  as a proxy for relative changes in rainfall amount. In the modern tropical cli-

matological setting of the western equatorial Pacific, the  $\delta^{18}$ O of precipitation decreases as precipitation amount increases (Cobb et al., 2007; Moerman et al., 2013). This "amount effect" (Dansgaard, 1964) forms the basis for past monsoon rainfall reconstructions from speleothem  $\delta^{18}$ O records across the region (Ayliffe et al., 2013; Carolin et al., 2013; Griffiths et al., 2009; Lewis et al., 2011; Partin et al., 2007). Temperature effects on the fractionation of oxygen isotopes in tropical precipitation are small (Dansgaard, 1964) and approximately negated by the opposing temperature-dependent fractionation of oxygen isotopes in cave calcite (Hendy and Wilson, 1968).

#### 3.2. Ice volume correction

Over glacial–interglacial time scales, changes in the volume of ice stored on land alter the  $\delta^{18}{\rm O}$  of seawater and resulting precipitation (Bintanja et al., 2005; Schrag et al., 1996; Waelbroeck et al., 2002). This means that an ice volume correction is necessary to examine relative changes in monsoon strength between the LGM and Holocene, along the lines of recent speleothem  $\delta^{18}{\rm O}$  studies (Ayliffe et al., 2013; Carolin et al., 2013). An ice volume correction was applied to all of the speleothem  $\delta^{18}{\rm O}$  records used in this study to account for the effects of changes in the  $\delta^{18}{\rm O}$  of seawater (Fig. 4).

To perform the ice volume correction, the speleothem  $\delta^{18}$ O time series were binned at 100-yr average resolution to ensure that the corrections were applied in the same way to all datasets. We use the record of Bintanja et al. (2005) for global seawater  $\delta^{18}$ O change (relative to the present day). This global seawater

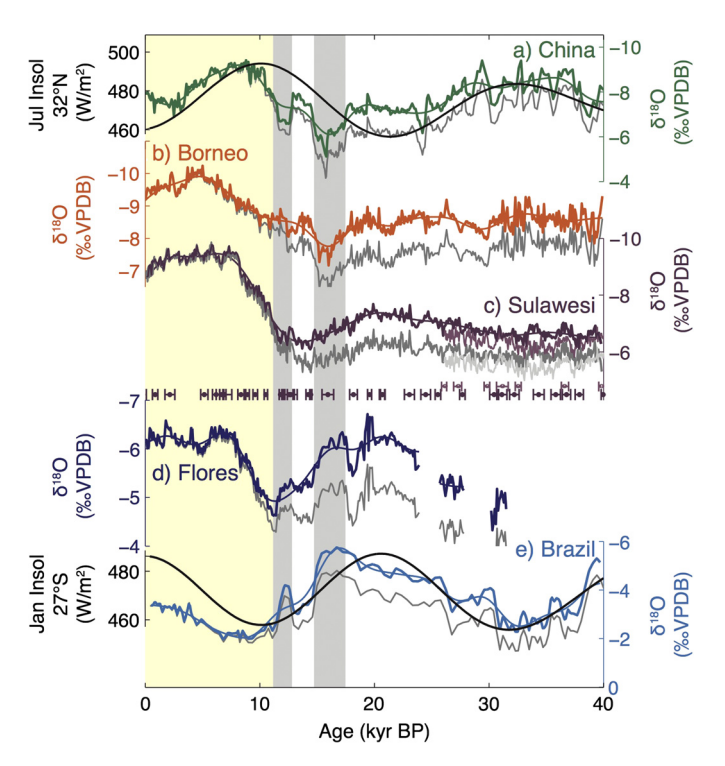


**Fig. 4. Speleothem**  $\delta^{18}$ **0 records.** (a) Hulu and Dongge caves, China (Dykoski et al., 2005; Wang et al., 2001) and July insolation at 32°N; (b) Gunung Buda National Park, Borneo (Carolin et al., 2013; Partin et al., 2007); (c) Sulawesi (this study); (d) Liang Luar Cave, Flores (Ayliffe et al., 2013; Griffiths et al., 2009; Lewis et al., 2011); (e) Botuverá Cave, Brazil (Wang et al., 2007) and January insolation at 27°S. All  $\delta^{18}$ O records have been corrected for ice-volume effects, with uncorrected data shown in grey. Thin coloured lines show the 25 kyr low pass filtered records used in Fig. 5a. The  $^{23}$ OTh dates (with  $\pm 2$  s.e. of mean) for Sulawesi are shown in purples (c). Grey shading highlights prominent weak monsoon intervals in China (Cheng et al., 2009) related to Heinrich Stadial 1 and the Younger Dryas. Yellow shading denotes the strong atmospheric convection interval in the MC.

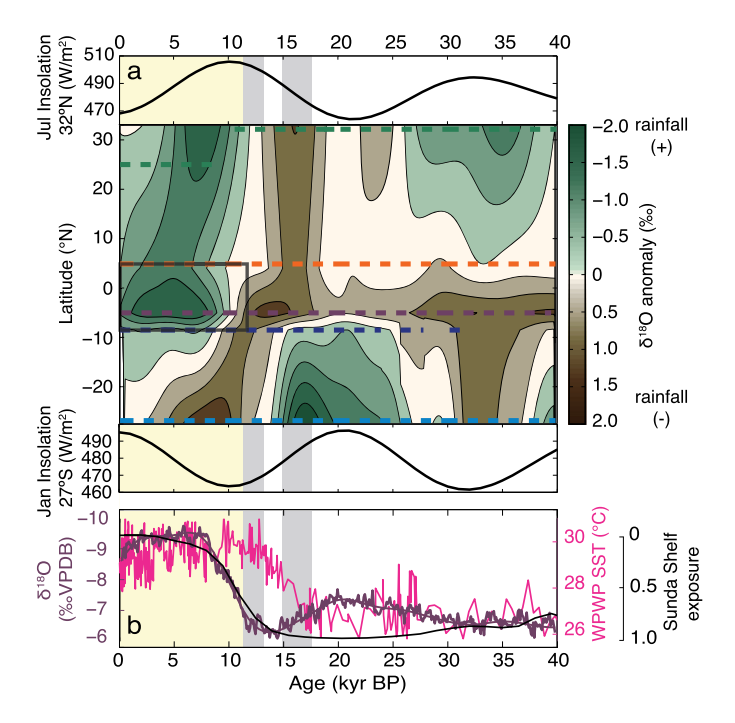


**Fig. 5. Orbital-scale palaeomonsoon changes over the last 40 kyr.** (a) Palaeomonsoon spatio-temporal reconstruction with summer insolation curves for 32°N (top) and 27°S (bottom). Dashed lines indicate the latitude and timespan of speleothem  $\delta^{18}$ O records used to construct the map (colours as for Fig. 4). The black box highlights the post-glacial increase in deep atmospheric convection over the MC. (b) Ice volume corrected GB09-3 speleothem  $\delta^{18}$ O record for Sulawesi (purple) shown with Mg/Ca summer SST for the Indo-Pacific Warm Pool (Stott et al., 2002) (pink) and fraction of Sunda Shelf exposed above sea level (bounded by 95°E–120°E and 10°S–10°N, derived from sea level data and elevation models; black) (Carolin et al., 2013). Grey and yellow shading as in Fig. 4.

 $\delta^{18}$ O record is routinely used to correct for the effects of ice volume changes on ice core temperature reconstructions (Jouzel et al., 2003; Stenni et al., 2010). We use a simple subtraction of the global ocean  $\delta^{18}$ O change to correct the speleothem records for ice volume effects (Ayliffe et al., 2013; Carolin et al., 2013), because of the expected retention of ocean  $\delta^{18}$ O changes in tropical rainfall (Jouzel et al., 2003).

## 3.3. Palaeomonsoon map

To qualitatively visualise broad-scale changes in Australasian monsoon hydroclimate over the last 40 kyr, we combine filtered speleothem  $\delta^{18}O$  records across a latitudinal transect (Fig. 4) to construct a palaeomonsoon map (Fig. 5). To isolate the precessionforced component of  $\delta^{18}\text{O}$  variability across the Australasian speleothem transect, a 25-kyr low-pass Butterworth filter was applied to each record to remove high-frequency variability. Oxygen isotope anomalies for each filtered record were calculated by subtracting the mean isotope value for the 23-0 kyr BP interval. This timeframe includes one complete precession cycle, ensuring that the normalisation includes both maximum and minimum local insolation values. It also represents the period of common data coverage for the records; ensuring anomalies are comparable among different records. The oxygen-isotope anomaly time-series were then plotted according to latitude and linearly interpolated to fill between the spatio-temporal transects of speleothem data. The strong chronological control provided by U-Th dating of the speleothem records means that age uncertainties for individual records is less than 500 yr (the largest age uncertainties over the last 40 kyr are for the record of Carolin et al., 2013).

Given the lack of precession-driven speleothem records for northern Australia, we instead choose to use a record from South America as the southern anchor for this analysis. There are a number of speleothem  $\delta^{18}{\rm O}$  records for South America (Cruz et al., 2005, 2009; Kanner et al., 2012; Wang et al., 2004, 2006, 2007) that could be used as the southern anchor for our study. Insolation-driven signals dominate the palaeomonsoon map, therefore we excluded records where insolation does not appear to have a strong influence on the record (Kanner et al., 2012). We also exclude discontinuous records (Wang et al., 2004, 2006) and records that do not span the entire period from 40 kyr BP to the present (Cruz et al., 2009). Based on these criteria, two records from Botuverá Cave in Brazil meet our data requirements (Cruz et al., 2005; Wang et al., 2007). Both records broadly agree on low-frequency features, but we selected the record of Wang et al. (2007) for the analysis because it has stronger chronological control over the last 40 kyr compared to the record of Cruz et al. (2005).

## 4. Discussion

# 4.1. Orbital timescales

This new spatio-temporal perspective reveals a striking disconnect between rainfall changes in the subtropical and equatorial regions of the Australasian monsoon domain. Anti-phased rainfall anomalies that follow precessional changes in mid-latitude summer insolation dominate the broad-scale patterns of northern and southern monsoon rainfall in the subtropics over the last 40 kyr (Fig. 5). In contrast, a dry background climate state dominates the core of the Australasian monsoon region prior to ~12 kyr BP.

Sulawesi, at 5°S, appears to lie near the centre of sustained, dry anomalies, with the low  $\delta^{18}$ O values (high rainfall) of the Holocene never achieved over the dry late glacial interval ( $\sim$ 12–40 kyr BP) in this record. Pervasive dry conditions at this time are a feature of other rainfall indicators from Sulawesi (Russell et al., 2014; Tierney et al., 2012) and the wider western equatorial Pacific region (DiNezio and Tierney, 2013; Dubois et al., 2014), and demonstrate that deep atmospheric convection over the western equatorial Pacific was suppressed during the late glacial interval.

The palaeomonsoon reconstruction provides a temporal context for previous spatial examinations (DiNezio and Tierney, 2013) of western equatorial Pacific hydroclimate at the Last Glacial Maximum (LGM). We find that the suppressed atmospheric convection over the western equatorial Pacific during the late glacial period ended abruptly with a step-wise increase in western equatorial Pacific rainfall into the Holocene. The rapid decrease in speleothem  $\delta^{18}$ O began at  $\sim$ 12 kyr BP in Sulawesi, and is recorded to a lesser extent in speleothems from Borneo and Flores (Fig. 4 and Fig. 5). Importantly, the main strengthening of deep convection over the western equatorial Pacific occurred too late to be triggered entirely by rising sea surface temperatures (Stott et al., 2002), which would have increased atmospheric moisture fluxes over the region (Fig. 5b). Instead, the two largest  $\delta^{18}\text{O}$  decreases in the Sulawesi record coincide with rapid flooding of the Sahul ( $\sim$ 12–11 kyr BP) and Sunda ( $\sim$ 8.5 kyr BP) shelves (Fig. 6). Event 1 occurs from 12-11 kyr BP during the flooding of the Sahul Shelf across the Gulf of Carpentaria (De Deckker et al., 2002; Reeves et al., 2008). Flooding event 2 occurs at around 8.5 kyr BP during the flooding of the Sunda Shelf. The timing of the flooding of the Sunda Shelf has been previously placed at approximately 9.5 kyr BP (Griffiths et al., 2013; Linsley et al., 2010). However, examination of these records reveals that the transition spans  $\sim$ 1 kyr, suggesting that the 8.5 kyr BP signal in the Sulawesi speleothem record is the same event (Fig. 6). These rapid changes in speleothem  $\delta^{18}O$  likely represent a combination of the reorganisation of local water masses, changes in source moisture pathways (Linsley et al., 2010) and intensification of the Walker circulation caused by enhanced convection over newly formed seas in

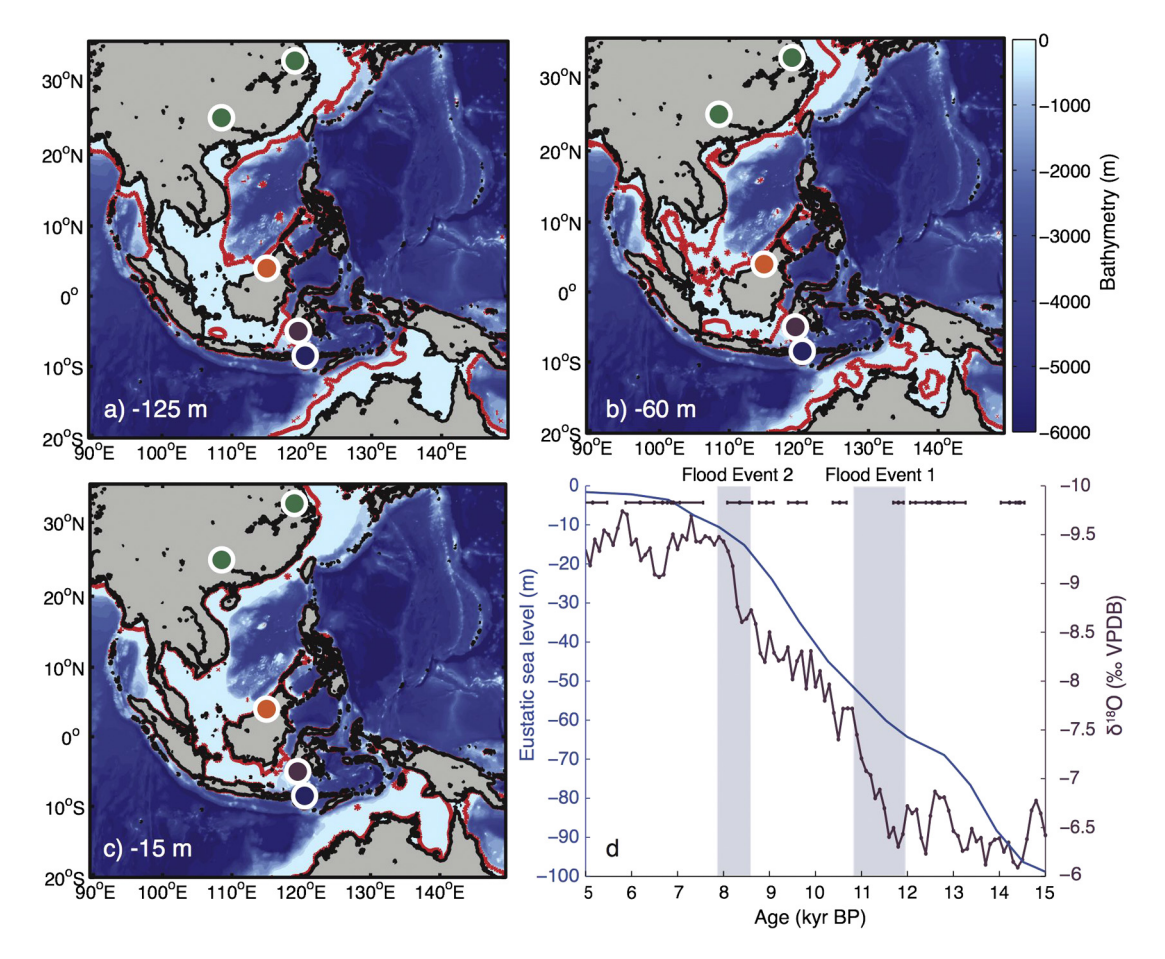


Fig. 6. Bathymetry of the IPWP and timing of continental shelf flooding events. (a) Bathymetry of the IPWP, with the -125 m contour in red, highlighting the sea level low stand during the LGM. (b) As for (a), but with the -60 m contour highlighting the approximate depth of the Sahul Shelf flooding. (c) As for (a) but with the -15 m contour highlighting the approximate depth of the Sunda Shelf flooding. Speleothem locations marked by coloured circles (colours as for Fig. 4). (d) Sulawesi flood events, plotted against regional eustatic sea level (Reeves et al., 2013).

the western equatorial Pacific region (DiNezio and Tierney, 2013; Griffiths et al., 2009; Tierney et al., 2012).

Consistent with our observations of suppressed atmospheric convection over the western equatorial Pacific during the late glacial period, an earlier spatial assessment of Indo-Pacific hydroclimate at the LGM found that its structure was best captured by simulations of the HadCM3 model, where exposure of the Sunda Shelf displaced the ascending branch of the Pacific Walker circulation to the east of Papua New Guinea (DiNezio and Tierney, 2013). The new Sulawesi record and palaeomonsoon map support the hypothesis that pervasive late-glacial dry conditions in the western equatorial Pacific were only terminated when deep atmospheric convection strengthened in response to rising sea levels and the inundation of shallow continental shelves in the region, well after the onset of deglaciation (DiNezio and Tierney, 2013; Griffiths et al., 2013).

A second prominent feature of the palaeomonsoon reconstruction is the interplay between orbital and millennial-scale climate forcing during deglaciation. The most southerly excursion of the ITCZ over the last 40 kyr occurred between  $\sim\!18$  and 15 kyr BP (Fig. 5). This period corresponds with Heinrich Stadial 1 (H1), which led to a weak monsoon interval in China (Cheng et al., 2009), enhanced monsoon rainfall in Flores (Ayliffe et al., 2013) (Fig. 4) and an extreme wet phase across northern Australia (Denniston et al., 2013; Muller et al., 2008). H1 occurred  $\sim\!4$  kyr after a Southern Hemisphere summer insolation maximum and during a time of near maximum Northern Hemisphere ice sheet extent. Together, these conditions cooled the Northern Hemisphere relative to the Southern Hemisphere and displaced the Australasian

monsoon to an extreme southerly position. A southward shift of latitudinal climate belts during H1 has been proposed as a key mechanism in the sequence of events leading to the release of carbon dioxide from the Southern Ocean during the onset of deglaciation (Anderson et al., 2009; Denton et al., 2010). The anomalous position of the Australasian monsoon during H1 documented here supports the hypothesis that a southward shift in the mean location of the ITCZ was critical for propagating Northern Hemisphere climate changes into the Southern Hemisphere during deglaciation.

# 4.2. Millennial-scale variability

To examine high-frequency variability across the Australasian monsoon domain, we subtracted the 25-kyr low-pass filtered records from the ice volume corrected speleothem  $\delta^{18}$ O records (Fig. 7). To compare variability between speleothem and ice core records, we subtracted the 25-kyr low-pass filtered records from published ice core  $\delta^{18}$ O records to produce a millennial-scale variability record for NGRIP. We examine glacial-interglacial changes in millennial-scale  $\delta^{18}$ O variability by determining the standard deviation of each filtered record in the 11–0 kyr BP interval and for the interval prior to 11 kyr BP (Fig. 7).

Strong latitudinal gradients are evident in the magnitude of millennial-scale hydroclimate variability across the Australasian monsoon domain (Fig. 7), with the largest changes in  $\delta^{18}$ O occurring at the northern and southern peripheries of the monsoon system. Here, latitudinal shifts in the mean location of the ITCZ in response to North Atlantic Heinrich and Dansgaard-Oeschger (D-O) climate events (NGRIP, 2004) influence the amount of rain-

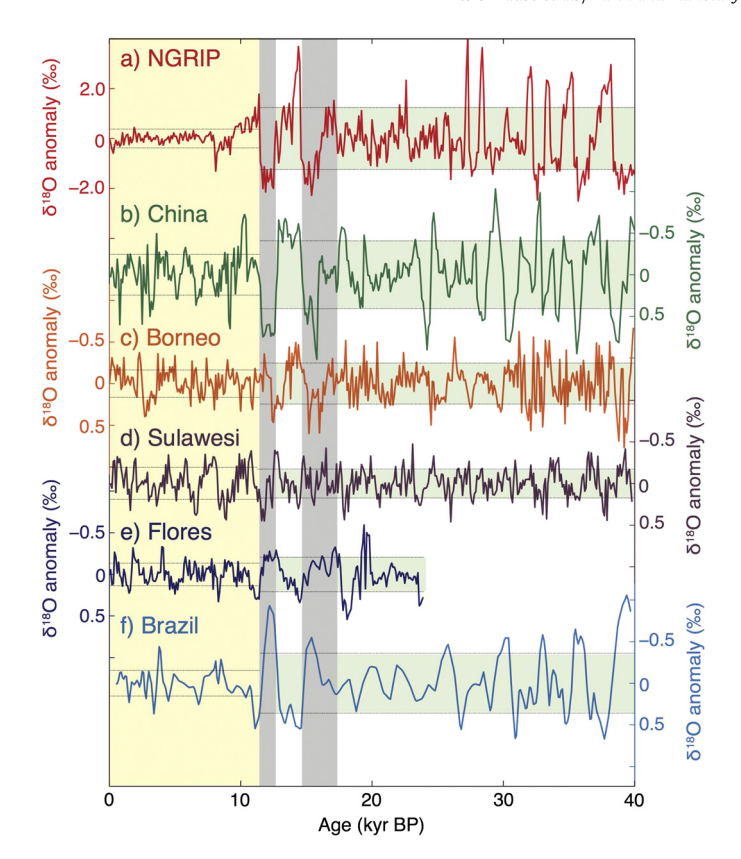


**Fig. 7. Millennial-scale palaeomonsoon variability over the last 40 kyr.** (a) NGRIP ice core (NGRIP, 2004), (b) China, (c) Borneo, (d) Sulawesi, (e) Flores and (f) Brazil  $\delta^{18}$ O anomalies after removing 25 kyr low pass filter. Horizontal lines and shading represent the  $\pm 1\sigma$  range in variability for the glacial (40–11 kyr BP; apart from (e) 24–11 kyr; green) and interglacial (11 kyr BP–present; yellow). Grey shading as in Fig. 4. Note that the y-axis  $\delta^{18}$ O scales are the same, except for NGRIP.

fall received. Consequently, markedly increased millennial-scale variability is observed in China (and Brazil) during the late glacial period when North Atlantic climate was highly variable compared to the more stable Holocene epoch (Dykoski et al., 2005; Wang et al., 2007, 2001) (Fig. 7). Across Australasia, the amplitude of millennial-scale  $\delta^{18}$ O excursions decreases toward the equator. Speleothems from Borneo (Carolin et al., 2013; Partin et al., 2007) and Flores (Ayliffe et al., 2013; Griffiths et al., 2009; Lewis et al., 2011) show an anti-phased rainfall response to Heinrich events, but weaker D-O events are not reliably observed. Neither Heinrich nor D-O events are evident in Sulawesi, and the millennial-scale  $\delta^{18}{\rm O}$  variability was similarly suppressed during the late glacial interval and the Holocene (Fig. 7). Together, these latitudinal gradients show that while North Atlantic Heinrich and D-O events caused marked shifts in the ITCZ and an associated rainfall seesaw at the peripheries of the Australasian monsoon, the strength of atmospheric convection and rainfall over the central western equatorial Pacific was less responsive to millennial-scale climate shifts.

Sulawesi at 5°S appears to lie at a fulcrum between hemispherically opposed rainfall anomalies experienced at the northern and southern limits of the Australasian monsoon. The millennial-scale climate stability in the core of the Australasian monsoon could be the outcome of the dry late glacial climate of the western equatorial Pacific, which may have reduced the capacity of millennial events to cause a measurable rainfall response (Fig. 4 and Fig. 7). The stability of western equatorial Pacific convection to millennial-scale forcing may also be a consequence of the broad latitudinal sweep of the ITCZ over the western equatorial Pacific region, with shifts in the position of the ITCZ influencing rainfall at its mar-

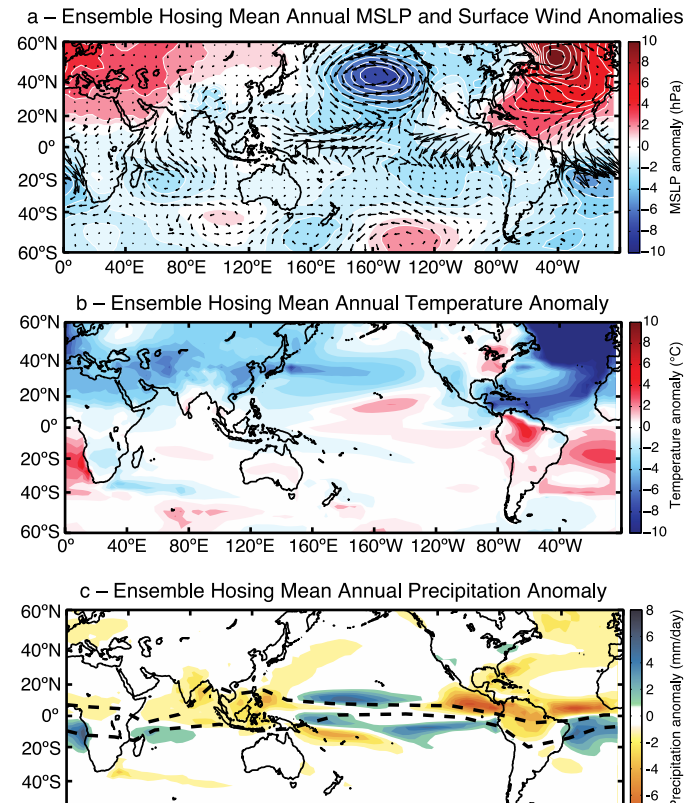


Fig. 8. Model ensemble hosing mean annual MSLP, surface wind, temperature and precipitation anomalies. (a) Hosing minus control ensemble mean annual MSLP and surface wind anomalies. (b) Hosing minus control ensemble mean annual surface air temperature anomalies. (c) Hosing minus control ensemble mean annual precipitation anomalies. The mean DJF and JJA ITCZ locations for the hosing runs are shown with dashed black lines. Anomalies are calculated using the ensemble mean (17 kyr, 24 kyr and 32 kyr) hosing and control values.

80°E 120°E 160°E 160°W 120°W 80°W 40°W

gins without affecting convective rainfall over the core western equatorial Pacific region. Alternatively, southward displacements of the ITCZ during millennial climate events may have caused Sulawesi to transition to a climate regime influenced by the Northern Hemisphere side of the Australasian monsoon. If so, any accompanying change in precipitation seasonality may not be recorded by the Sulawesi speleothems because the nearby mountainous barrier restricts rainfall reaching the cave site during boreal summer (Fig. 1b).

# 4.3. Model comparison

We explored the muted sensitivity of MC rainfall to millennial-scale events by simulating the seasonal pattern of rainfall anomalies for the three most recent Heinrich events (H1, H2 and H3) using the HadCM3 general circulation model (Singarayer and Valdes, 2010). The ensemble control simulation (mean of 17, 24 and 32 kyr BP control runs; i.e. without hosing applied) shows a 6°C global average cooling, with the largest cooling over the North American Laurentide Ice Sheet (Fig. 8). There is a small reduction in the global rate of precipitation, centred over the IPWP due to a weakening of the Australasian monsoon, in agreement with proxy records (DiNezio and Tierney, 2013) and the palaeomonsoon map (Fig. 4, Fig. 5).

Hosing results from HadCM3 compare well with similar hosing experiments from the Community Climate System Model 3 (CCSM3), with the spatial patterns of temperature and precipitation anomalies very similar between models (Mohtadi et al., 2014).

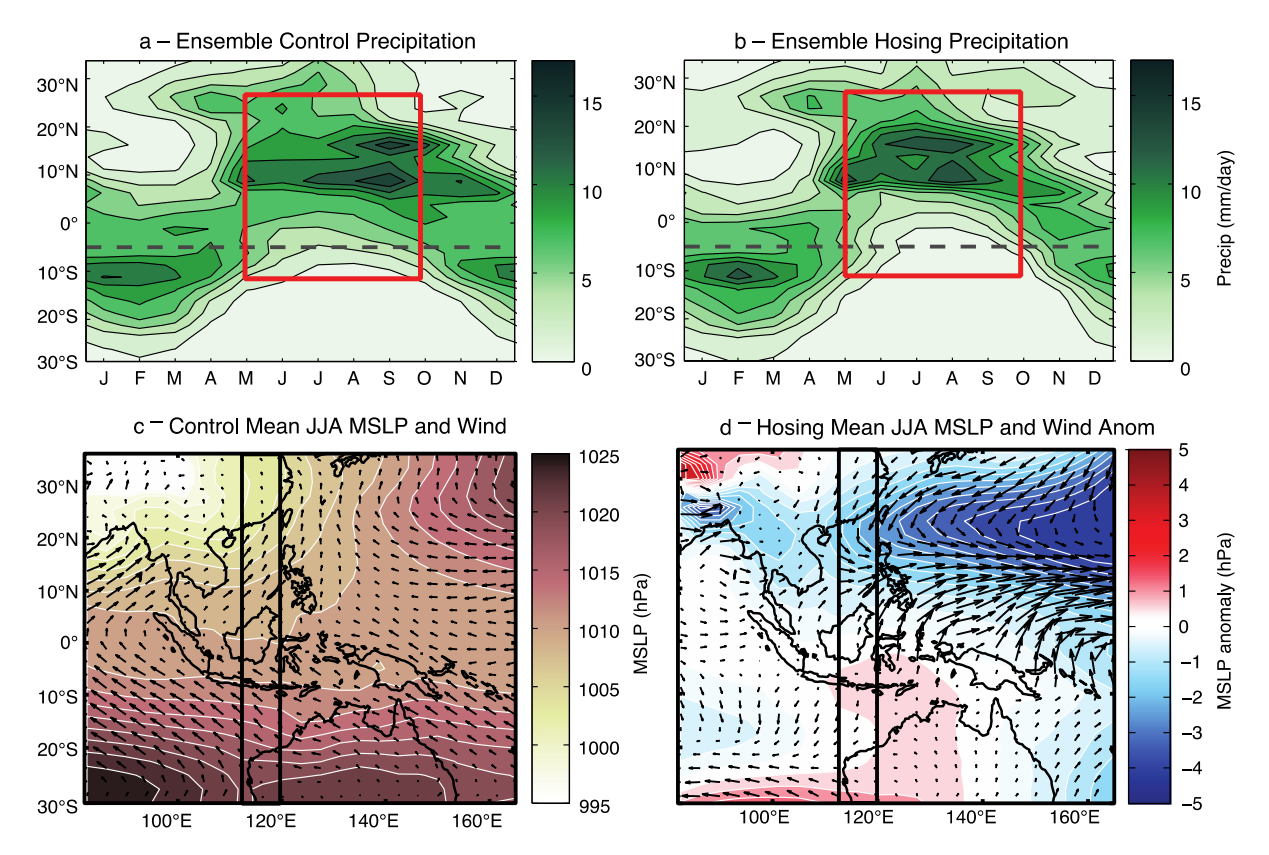


**Fig. 9. Modelled rainfall seasonality transect over the IPWP.** Rainfall seasonality averaged longitudinally over a latitudinal transect (116–120°E; shown in panels c and d) for (a) the control, and (b) the hosing ensembles, calculated as the mean values for the 17 kyr, 24 kyr and 32 kyr runs. Red boxes highlight the seasonal anomalies during boreal summer. Mean rainfall for each month was calculated for the transect and plotted to produce a spatio-temporal map of rainfall seasonality across the IPWP. The latitude of Sulawesi is given by a dashed line. (c) Mean JJA MSLP and surface winds averaged for the control ensemble. (d) Mean JJA MSLP and surface wind anomalies for the hosing ensemble

CCSM3 shows a clear southward shift of the ITCZ over the Indian Ocean, resulting from a weakening of the southern Indian Ocean Hadley circulation. This result is mirrored in HadCM3, demonstrated by northerly wind anomalies across the equatorial Indian Ocean (Fig. 8). The comparable results for Heinrich events across the Indian Ocean achieved by the HadCM3 and CCSM3 simulations gives confidence to the skill of the HadCM3 model in simulating a reproducible response to a simulated Heinrich event.

Hosing of the North Atlantic Ocean results in a marked cool anomaly over the North Atlantic, due to the dramatic reduction of the strength of the Atlantic Meridional Overturning Circulation (Fig. 8b). The South Atlantic subsequently warms due to the establishment of a bipolar seesaw, and the ITCZ over the Atlantic shifts south. Anomalies in the North Atlantic are propagated into the eastern Pacific Ocean by anomalous easterly winds, moving across the Isthmus of Panama (Fig. 8a). A temperature dipole is established in the eastern Pacific, with cool temperature anomalies north of the equator, and warm anomalies south of the equator, causing a southward shift of the ITCZ in this region (Fig. 8; Note that HadCM3 is known to exhibit a 'double ITCZ' (e.g. Bellucci et al., 2010)). The north Pacific trade winds weakened, with anomalous westerly winds over the western Pacific, and a net drying over the IPWP.

The seasonality of precipitation across a latitudinal transect of the MC was examined through the production of spatio-temporal precipitation anomaly maps. A longitudinally averaged, latitudinal transect of the MC (35°N to 20°S, 116 to 120°E) was calculated for each month to produce a spatial map of the seasonally evolving precipitation distribution across the MC (Fig. 9). When forced with freshwater hosing of the North Atlantic, rainfall seasonality at Sulawesi is enhanced for all three simulated H events (Fig. 9).

The larger seasonal range at Sulawesi is the result of a decline in rainfall during ~June-September (the local dry season), with no accompanying change in austral summer monsoon rainfall. This asymmetry of the seasonal pattern is caused by a simulated narrowing of the width of the ITCZ over the MC during boreal summer; a result of southerly winds pushing northwards over the MC toward an anomalous low-pressure cell in the North Pacific (Fig. 8, Fig. 9). This result is consistent with that of Zhang et al., 2018, which models a strong precipitation anomaly in boreal summer over China with Community Earth System Model (CESM). The simulated decline in ∼June-September rainfall in the HadCM3 experiments suggests that, on average, the Northern Hemisphere drying during H events might have extended south to Sulawesi, in-phase with the rainfall response in Borneo. Future research targeting palaeoclimate records from southern locations within the MC that are sensitive to the austral winter monsoon would be valuable in assessing the changes in ITCZ positioning produced in model hosing experiments.

#### 5. Conclusion

Our palaeomonsoon reconstruction highlights the different processes that drive spatial and temporal rainfall variability across the Australasian monsoon domain. In Sulawesi, glacial-interglacial variations in MC continental shelf exposure influence the intensity of deep atmospheric convection over the centre of the MC (Meckler et al., 2012). In contrast, precession-dominated modulation of rainfall is largely restricted to the northern and southern peripheries of the Australasian monsoon domain. On millennial scales, the latitudinal response of the Australasian monsoon decreases toward the core of the MC region, culminating in a lack

of expression in the Sulawesi record. Model results suggest that during millennial-scale events, the seasonality of rainfall across the MC region changes most markedly during the boreal summer; however the strong austral summer seasonality of our record means that no change is seen in the Sulwesi speleothem record. Taken together, our findings demonstrate that glacial-interglacial changes in northern ice sheets drive the intensity of deep atmospheric convection over the MC, whereas North Atlantic millennial-scale climate change serves to redistribute monsoon rainfall latitudinally and seasonally across Australasia.

**Data archiving.** The Sulawesi speleothem data reported in this paper are archived at the NOAA World Data Center for Paleoclimatology.

#### Acknowledgements

The project was carried out in Indonesia under Kementerian Negara Riset dan Teknologi (RISTEK) research permit numbers 04/TKPIPA/FRP/SM/IV/2009 and 1b/TKPIPA/FRP/SM/I/2011. We thank the Research Center for Geotechnology, Indonesian Institute of Sciences (LIPI) for logistical support and are indebted to Neil Anderson, Dan Zwartz, Garry Smith, Linda Ayliffe, Nick Scroxton, Engkos Kosasih, Djupriono and the staff of Bantimurung-Bulusaraung National Park (with special thanks to Syaiful Fajrin) for their invaluable technical assistance in the field. We also thank Heather Scott-Gagan, Joan Cowley, Joe Cali and Daniel Becker for laboratory assistance, and Paul Valdes, Joy Singarayer and Peter Hopcroft for providing the HadCM3 simulations for analysis.

This study was supported by Australian Research Council (ARC) Discovery grants DP0663274 and DP1095673 to M.K.G., J.C.H., W.S.H., R.L.E, and H.C.; an Australian Postgraduate Award to C.E.K.; an ARC Future Fellowship to J.C.H. (FT130100801); an ARC Queen Elizabeth II fellowship to N.J.A. (DP110101161); U.S. NSF grants (1103402) and (1702816) to R.L.E. and H.C.; and National Natural Science Foundation of China grants to H.C. (NSFC 41731174 and 41888101).

# Appendix A. Supplementary material

Supplementary material related to this article can be found online at https://doi.org/10.1016/j.epsl.2019.01.045.

# References

- Anderson, R.F., Ali, S., Bradtmiller, L.I., Nielsen, S.H.H., Fleisher, M.Q., Anderson, B.E., Burckle, L.H., 2009. Wind-driven upwelling in the Southern Ocean and the deglacial rise in atmospheric CO<sub>2</sub>. Science 323, 1443–1448.
- Ayliffe, L.K., Gagan, M.K., Zhao, J.-x., Drysdale, R.N., Hellstrom, J.C., Hantoro, W.S., Griffiths, M.L., Scott-Gagan, H., St Pierre, E., Cowley, J.A., Suwargadi, B.W., 2013. Rapid interhemispheric climate links via the Australasian monsoon during the last deglaciation. Nat. Commun. 4, 2908.
- Bellucci, A., Gualdi, S., Navarra, A., 2010. The double-ITCZ syndrome in coupled general circulation models: the role of large-scale vertical circulation regimes. J. Climate 23. 1127–1145.
- Bintanja, R., van de Wal, R.S.W., Oerlemans, J., 2005. Modelled atmospheric temperatures and global sea levels over the past million years. Nature 437, 125–128.
- Carolin, S.A., Cobb, K.M., Adkins, J.F., Clark, B., Conroy, J.L., Lejau, S., Malang, J., Tuen, A.A., 2013. Varied response of Western Pacific hydrology to climate forcings over the Last Glacial period. Science 340, 1564–1566.
- Cheng, H., Edwards, R.L., Broecker, W.S., Denton, G.H., Kong, X., Wang, Y., Zhang, R., Wang, X., 2009. Ice age terminations. Science 326, 248–252.
- Chiang, J.C.H., 2009. The tropics in paleoclimate. Annu. Rev. Earth Planet. Sci. 37, 263–297.
- Cobb, K.M., Adkins, J.F., Partin, J.W., Clark, B., 2007. Regional-scale climate influences on temporal variations of rainwater and cave dripwater oxygen isotopes in northern Borneo. Earth Planet. Sci. Lett. 263, 207–220.
- Cruz, F.W., Burns, S.J., Karmann, I., Sharp, W.D., Vuille, M., Cardoso, A.O., Ferrari, J.A., Silva Dias, P.L., Viana Jr, O., 2005. Insolation-driven changes in atmospheric circulation over the past 116,000 years in subtropical Brazil. Nature 434, 63–66.

- Cruz, F.W., Vuille, M., Burns, S.J., Wang, X., Cheng, H., Werner, M., Edwards, R.L., Karmann, I., Auler, A.S., Nguyen, H., 2009. Orbitally driven east-west antiphasing of South American precipitation. Nat. Geosci. 2, 210–214.
- Dansgaard, W., 1964. Stable isotopes in precipitation. Tellus 16, 436-468.
- De Deckker, P., Tapper, N.J., van der Kaars, S., 2002. The status of the Indo-Pacific Warm Pool and adjacent land at the Last Glacial Maximum. Glob. Planet. Change 35, 25–35.
- Denniston, R.F., Wyrwoll, K.-H., Asmerom, Y., Polyak, V.J., Humphreys, W.F., Cugley, J., Woods, D., LaPointe, Z., Peota, J., Greaves, E., 2013. North Atlantic forcing of millennial-scale Indo-Australian monsoon dynamics during the Last Glacial period. Quat. Sci. Rev. 72, 159–168.
- Denton, G.H., Anderson, R.F., Toggweiler, J.R., Edwards, R.L., Schaefer, J.M., Putnam, A.E., 2010. The Last Glacial termination. Science 328, 1652–1656.
- Deschamps, P., Durand, N., Bard, E., Hamelin, B., Camoin, G., Thomas, A.L., Henderson, G.M., Okuno, J.i., Yokoyama, Y., 2012. Ice-sheet collapse and sea-level rise at the Bølling warming 14,600 years ago. Nature 483, 559–564.
- DiNezio, P.N., Tierney, J.E., 2013. The effect of sea level on glacial Indo-Pacific climate. Nat. Geosci. 6, 485–491.
- Dubois, N., Oppo, D.W., Galy, V.V., Mohtadi, M., van der Kaars, S., Tierney, J.E., Rosenthal, Y., Eglinton, T.I., Lückge, A., Linsley, B.K., 2014. Indonesian vegetation response to changes in rainfall seasonality over the past 25,000 years. Nat. Geosci. 7, 513–517.
- Dykoski, C.A., Edwards, R.L., Cheng, H., Yuan, D., Cai, Y., Zhang, M., Lin, Y., Qing, J., An, Z., Revenaugh, J., 2005. A high-resolution, absolute-dated Holocene and deglacial Asian monsoon record from Dongge Cave, China. Earth Planet. Sci. Lett. 233, 71–86
- Fairbanks, R.G., 1989. A 17,000-year glacio-eustatic sea level record: influence of glacial melting rates on the Younger Dryas event and deep-ocean circulation. Nature 342, 637–642.
- Griffiths, M.L., Drysdale, R.N., Gagan, M.K., Zhao, J.-x., Ayliffe, L.K., Hellstrom, J.C., Hantoro, W.S., Frisia, S., Feng, Y., Cartwright, I., St Pierre, E., Fischer, M.J., Suwargadi, B.W., 2009. Increasing Australian–Indonesian monsoon rainfall linked to early Holocene sea-level rise. Nat. Geosci. 2, 636–639.
- Griffiths, M.L., Drysdale, R.N., Gagan, M.K., Zhao, J.-x., Hellstrom, J.C., Ayliffe, L.K., Hantoro, W.S., 2013. Abrupt increase in east Indonesian rainfall from flooding of the Sunda Shelf ~9500 years ago. Quat. Sci. Rev. 74, 273–279.
- Hellstrom, J.C., 2003. Rapid and accurate U/Th dating using parallel ion-counting multi-collector ICP-MS. J. Anal. At. Spectrom. 18, 1346–1351.
- Hellstrom, J.C., 2006. U-Th dating of speleothems with high initial <sup>230</sup>Th using stratigraphical constraint. Quat. Geochronol. 1, 289–295.
- Hendy, C.H., Wilson, A.T., 1968. Palaeoclimatic data from speleothems. Nature 219, 48–51.
- Jouzel, J., Vimeux, F., Caillon, N., Delaygue, G., Hoffmann, G., Masson-Delmotte, V., Parrenin, F., 2003. Magnitude of isotope/temperature scaling for interpretation of central Antarctic ice cores. J. Geophys. Res. 108, 4361.
- Kageyama, M., Merkel, U., Otto-Bliesner, B., Prange, M., Abe-Ouchi, A., Lohmann, G., Ohgaito, R., Roche, D.M., Singarayer, J., Swingedouw, D., Zhang, X., 2013. Climatic impacts of fresh water hosing under Last Glacial Maximum conditions: a multi-model study. Clim. Past 9, 935–953.
- Kanner, L.C., Burns, S.J., Cheng, H., Edwards, R.L., 2012. High-latitude forcing of the South American Summer Monsoon during the last glacial. Science 335, 570–573.
- Lewis, S.C., Gagan, M.K., Ayliffe, L.K., Zhao, J.-x., Hantoro, W.S., Treble, P.C., Hellstrom, J.C., LeGrande, A.N., Kelley, M., Schmidt, G.A., Suwargadi, B.W., 2011. High-resolution stalagmite reconstructions of Australian–Indonesian monsoon rainfall variability during Heinrich stadial 3 and Greenland interstadial 4. Earth Planet. Sci. Lett. 303, 133–142.
- Linsley, B.K., Rosenthal, Y., Oppo, D.W., 2010. Holocene evolution of the Indonesian throughflow and the western Pacific warm pool. Nat. Geosci. 3, 578–583.
- Meckler, A.N., Clarkson, M.O., Cobb, K.M., Sodemann, H., Adkins, J.F., 2012. Interglacial hydroclimate in the tropical west Pacific through the late Pleistocene. Science 336, 1301–1304.
- Moerman, J.W., Cobb, K.M., Adkins, J.F., Sodemann, H., Clark, B., Tuen, A.A., 2013. Diurnal to interannual rainfall  $\delta^{18}$ O variations in northern Borneo driven by regional hydrology. Earth Planet. Sci. Lett. 369–370, 108–119.
- Mohtadi, M., Prange, M., Oppo, D.W., De Pol-Holz, R., Merkel, U., Zhang, X., Steinke, S., Lückge, A., 2014. North Atlantic forcing of tropical Indian Ocean climate. Nature 509, 76–80.
- Muller, J., Kylander, M., Wüst, R.A.J., Weiss, D., Martinez-Cortizas, A., LeGrande, A.N., Jennerjahn, T., Behling, H., Anderson, W.T., Jacobson, G., 2008. Possible evidence for wet Heinrich phases in tropical NE Australia: the Lynch's Crater deposit. Quat. Sci. Rev. 27, 468–475.
- NGRIP, 2004. High-resolution record of Northern Hemisphere climate extending into the last interglacial period. Nature 431, 147–151.
- Partin, J.W., Cobb, K.M., Adkins, J.F., Clark, B., Fernandez, D.P., 2007. Millennial-scale trends in west Pacific warm pool hydrology since the Last Glacial Maximum. Nature 449, 452–455.
- Reeves, J.M., Bostock, H.C., Ayliffe, L.K., Barrows, T.T., De Deckker, P., Devriendt, L.S., Dunbar, G.B., Drysdale, R.N., Fitzsimmons, K.E., Gagan, M.K., Griffiths, M.L., Haberle, S.G., Jansen, J.D., Krause, C., Lewis, S., McGregor, H.V., Mooney, S.D., Moss, P., Nanson, G.C., Purcell, A., van der Kaars, S., 2013. Palaeoenvironmental

- change in tropical Australasia over the last 30,000 years a synthesis by the OZ-INTIMATE group. Quat. Sci. Rev. 74, 97–114.
- Reeves, J.M., Chivas, A.R., García, A., Holt, S., Couapel, M.J.J., Jones, B.G., Cendón, D.I., Fink, D., 2008. The sedimentary record of palaeoenvironments and sea-level change in the Gulf of Carpentaria, Australia, through the last glacial cycle. Quat. Int. 183, 3–22.
- Russell, J.M., Vogel, H., Konecky, B.L., Bijaksana, S., Huang, Y., Melles, M., Wattrus, N., Costa, K., King, J.W., 2014. Glacial forcing of central Indonesian hydroclimate since 60,000 y B.P. Proc. Natl. Acad. Sci. 111, 5100.
- Schneider, T., Bischoff, T., Haug, G.H., 2014. Migrations and dynamics of the intertropical convergence zone. Nature 513, 45–53.
- Schrag, D.P., Hampt, G., Murray, D.W., 1996. Pore fluid constraints on the temperature and oxygen isotopic composition of the glacial ocean. Science 272, 1930–1932.
- Singarayer, J.S., Valdes, P.J., 2010. High-latitude climate sensitivity to ice-sheet forcing over the last 120 kyr. Quat. Sci. Rev. 29, 43–55.
- Stenni, B., Masson-Delmotte, V., Selmo, E., Oerter, H., Meyer, H., Röthlisberger, R., Jouzel, J., Cattani, O., Falourd, S., Fischer, H., Hoffmann, G., Iacumin, P., Johnsen, S.J., Minster, B., Udisti, R., 2010. The deuterium excess records of EPICA Dome C and Dronning Maud Land ice cores (East Antarctica). Quat. Sci. Rev. 29, 146–159.
- Stott, L., Poulsen, C., Lund, S., Thunell, R., 2002. Super ENSO and global climate oscillations at millennial time scales. Science 297, 222–226.
- Stouffer, R.J., Yin, J., Gregory, J.M., Dixon, K.W., Spelman, M.J., Hurlin, W., Weaver, A.J., Eby, M., Flato, G.M., Hasumi, H., Hu, A., Jungclaus, J.H., Kamenkovich, I.V., Levermann, A., Montoya, M., Murakami, S., Nawrath, S., Oka, A., Peltier, W.R., Robitaille, D.Y., Sokolov, A., Vettoretti, G., Weber, S.L., 2006. Investigating the causes of the response of the thermohaline circulation to past and future climate changes. J. Climate 19, 1365–1387.

- Tierney, J.E., Oppo, D.W., LeGrande, A.N., Huang, Y., Rosenthal, Y., Linsley, B.K., 2012. The influence of Indian Ocean atmospheric circulation on Warm Pool hydroclimate during the Holocene epoch. J. Geophys. Res. 117, D19108.
- Waelbroeck, C., Labeyrie, L., Michel, E., Duplessy, J.C., McManus, J.F., Lambeck, K., Balbon, E., Labracherie, M., 2002. Sea-level and deep water temperature changes derived from benthic foraminifera isotopic records. Quat. Sci. Rev. 21, 295–305.
- Wang, X., Auler, A.S., Edwards, R.L., Cheng, H., Cristalli, P.S., Smart, P.L., Richards, D.A., Shen, C.-C., 2004. Wet periods in northeastern Brazil over the past 210 kyr linked to distant climate anomalies. Nature 432, 740–743.
- Wang, X., Auler, A.S., Edwards, R.L., Cheng, H., Ito, E., Solheid, M., 2006. Interhemispheric anti-phasing of rainfall during the last glacial period. Quat. Sci. Rev. 25, 3391–3403.
- Wang, X., Auler, A.S., Edwards, R.L., Cheng, H., Ito, E., Wang, Y., Kong, X., Solheid, M., 2007. Millennial-scale precipitation changes in southern Brazil over the past 90,000 years. Geophys. Res. Lett. 34, L23701.
- Wang, Y.J., Cheng, H., Edwards, R.L., An, Z.S., Wu, J.Y., Shen, C.-C., Dorale, J.A., 2001.
  A high-resolution absolute-dated Late Pleistocene monsoon record from Hulu Cave, China. Science 294, 2345–2348.
- Webster, P.J., 1994. The role of hydrological processes in ocean–atmosphere interactions. Rev. Geophys. 32, 427–476.
- Webster, P.J., Magaña, V.O., Palmer, T.N., Shukla, J., Tomas, R.A., Yanai, M., Yasunari, T., 1998. Monsoons: processes, predictability, and the prospects for prediction. J. Geophys. Res. 103, 14451–14510.
- Zhang, H., Griffiths, M.L., Chiang, J.C.H., Kong, W., Wu, S., Atwood, A., Huang, J., Cheng, H., Ning, Y., Xie, S., 2018. East Asian hydroclimate modulated by the position of the westerlies during Termination I. Science 362, 580–583.